Inorganic Chemistry

FORUM ARTICLE

pubs.acs.org/IC

Metal-Stabilized Thiyl Radicals as Scaffolds for Reversible Alkene Addition via C−S Bond Formation/Cleavage

Kagna Ouch, Mark S. Mashuta, and Craig A. Grapperhaus*

Department of Chemistry, University of Louisville, Louisville, Kentucky 40292, United States

Supporting Information

ABSTRACT: The one-electron oxidation of metal thiolates results in an increased oxidation state of the metal ion or the formation of a sulfur-based, thiyl radical in limiting extremes. For complexes with highly covalent M−S bonds, the unpaired electron may be delocalized over the metal and the sulfur, yielding a metal-stabilized thiyl radical. Oxidation of the metal thiolate precursors $[Ru(DPPBT)_3]^-$, $[\mathbf{Ru\text{-}1}]^-$, and $Re(DPPBT)_3$, **Re-1** (DPPBT = diphenylphosphinobenzenethiolate), generates metal-stabilized thiyl radicals that react with alkenes to yield dithioether−metal products. Alkene addition to $[\mathbf{Ru\text{-}1}]^+$ and $[\mathbf{Re\text{-}1}]^+$ is symmetry-allowed due to the meridional arrangement of the DPPBT chelates. Combined bulk electrolysis and cyclic voltammetry experiments reveal the addition of alkenes to $[\mathbf{Ru\text{-}1}]^+$ as an irreversible process with experimentally determined rate constants ranging from $4.6(5) \times 10^7\ M^{-1}\ s^{-1}$ for electron-rich alkenes to $2.7(2) \times 10^4\ M^{-1}\ s^{-1}$ for electron-poor alkenes. Rate constants for cyclic alkenes range from $4(2) \times 10^7$ to $2.9(3) \times 10^3\ M^{-1}\ s^{-1}$. Chemical oxidation of $[\mathbf{Ru\text{-}1}]^-$ by ferrocenium hexafluorophosphate ($FcPF_6$) in the presence of *m*-methylstyrene or *p*-methylstyrene yields the dithioether complexes $[\mathbf{Ru\text{-}1 \cdot}\textit{\textbf{m}}\mathbf{\text{-methylstyrene}}]^+$ and $[\mathbf{Ru\text{-}1 \cdot}\textit{\textbf{p}}\mathbf{\text{-methylstyrene}}]^+$, respectively. Each complex was crystallized and the structure determined by single-crystal X-ray diffraction. ^{31}P NMR of the samples reveals a major and minor product, each displaying a second-order spectrum. The oxidized intermediate $[\mathbf{Re\text{-}1}]^+$ binds alkenes reversibly with equilibrium binding constants that vary with the complex charge from $1.9 \times 10^{-11}\ M^{-1}$ for $n = 0$ to $4.0\ M^{-1}$ for $n = +1$ to $2.5 \times 10^9\ M^{-1}$ for $n = +2$. The three binding regimes are separated by 240 mV. Crystalline samples of $[\mathbf{Re\text{-}1 \cdot C_2H_4}]^{2+}$ are obtained upon chemical oxidation of **Re-1** with silver hexafluorophosphate ($AgPF_6$) in the presence of ethylene. Strategies for the addition of alkenes to other metal-stabilized thiyl radicals are suggested.

INTRODUCTION

This Forum Article highlights recent efforts in our group toward the reversible addition of alkenes to metal-stabilized thiyl radicals via carbon−sulfur bond formation/cleavage reactions. As defined below, metal-stabilized thiyl radicals are discrete oxidation products of metal complexes with "noninnocent" thiolate ligands. They belong to a general class of reaction products that may be obtained upon air oxidation of metal−thiolate complexes, Scheme 1. Air oxidation of metal−thiolates can proceed through multiple steps including one- or two-electron events that are ligand- or metal-centered. Two-electron oxidations involve O-atom transfer, leading to high-valent metal oxo complexes[1,2] or metal-coordinated sulfur−oxygenates[3−6] with relevance to cysteine dioxygenase,[7,8] nitrile hydratase,[4,6,9−11] and thiocyanate hydrolase.[4,6,9,12] One-electron oxidations yield oxidized metal ions or thiyl radicals,[13−20] which may yield disulfide if not stabilized.

In this microreview, we focus on one-electron oxidations by electrochemical methods or through the use of oxygen-free chemical oxidants. In the simplest terms, the site of oxidation depends on the composition of the molecular orbital that loses an electron, Scheme 2. Molecular orbitals that are heavily localized toward the metal or the sulfur yield the corresponding oxidized metal or thiyl radical, accordingly. In cases where the orbital is nearly equally distributed between the metal and sulfur, a specific site of oxidation cannot be defined, as the unpaired electron is delocalized over both sites. We refer to these complexes as metal-stabilized thiyl radicals.

Potential precursors of metal-stabilized thiyl radicals include metal−thiolate complexes with highly nucleophilic sulfur centers. The nucleophilicity of metal−thiolates was attributed to repulsive metal−sulfur $d\pi$−$p\pi$ interactions by Enemark and Ashby more than 20 years ago.[21] More recently, we noted that metal−thiolates with nearly equal metal and sulfur character in the highest occupied molecular orbital (HOMO) display enhanced nucleophilicity as compared to those with higher sulfur character.[22−24] The oxidation of such complexes is likely to lead to metal-stabilized thiyl radicals.

The addition of organic thiyl radicals to unsaturated hydrocarbons is well established with applications including cis/trans isomerization, sulfide synthesis, and polymerization.[25−28] As a result, we elected to pursue the reactivity of metal-stabilized thiyl radicals with alkenes. This work was largely inspired by the reversible binding of ethylene to nickel−dithiolenes as a potential method for alkene purification reported by Wang and

Received: February 28, 2011
Published: May 25, 2011

ACS Publications © 2011 American Chemical Society

Scheme 1. Oxygen Sensitivity of Metal−Thiolates

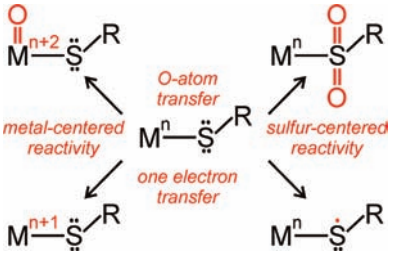

Scheme 2. Effect of Relative Metal and Sulfur Orbital Energies on the Site of Oxidation

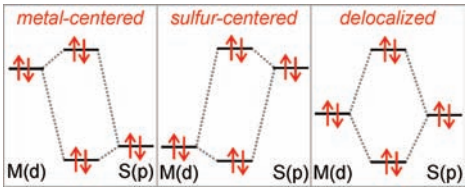

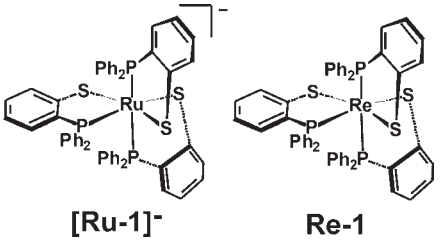

Figure 1. Stick representations of the metal−thiolate precursor complexes [**Ru-1**]$^-$ and **Re-1**.

Stiefel.[29] Later studies by Fekl et al.[30] and Geiger[31] independently showed complications with the oxidation induced C−S bond forming step and the reduction promoted C−S bond cleavage. Nevertheless, the concept of reversible, redox-controlled binding of alkenes to a metal−thiolate precursor remained intriguing. Through a series of recent studies, Fekl et al. obtained ethylene addition products with molybdenum dithiolenes that partially release the alkene in refluxing chloroform[32] and diene addition to platinum dithiolenes upon oxidation.[33] Also of note, Webster and co-workers reported alkene addition to a ruthenium thiolate upon chemical oxidation.[34] In the following pages, we will describe efforts from our group to develop a system for redox-controlled, reversible binding of unsaturated hydrocarbons to metal-stabilized thiyl radicals.

METAL-STABILIZED THIYL RADICALS

Our investigations with metal-stabilized thiyl radicals have largely focused on the Ru and Re complexes [Ru(DPPBT)$_3$]$^-$, [**Ru-1**]$^-$, and Re(DPPBT)$_3$, **Re-1** (DPPBT = diphenylphosphinobenzenethiolate), initially reported by Dilworth et al., Figure 1.[35,36] Regarding the multiple redox events of **Re-1**, Dilworth et al. noted that the ligand must "delocalize electron density in an analogous manner to dithiolenes".[35] We became further interested in these complexes due to the reported solvent-dependent

Scheme 3. Selected Reactions of [Ru-1]$^-$

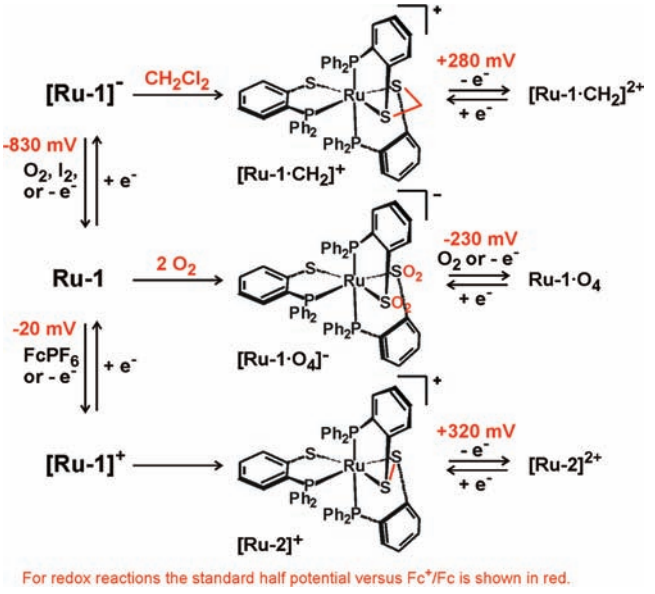

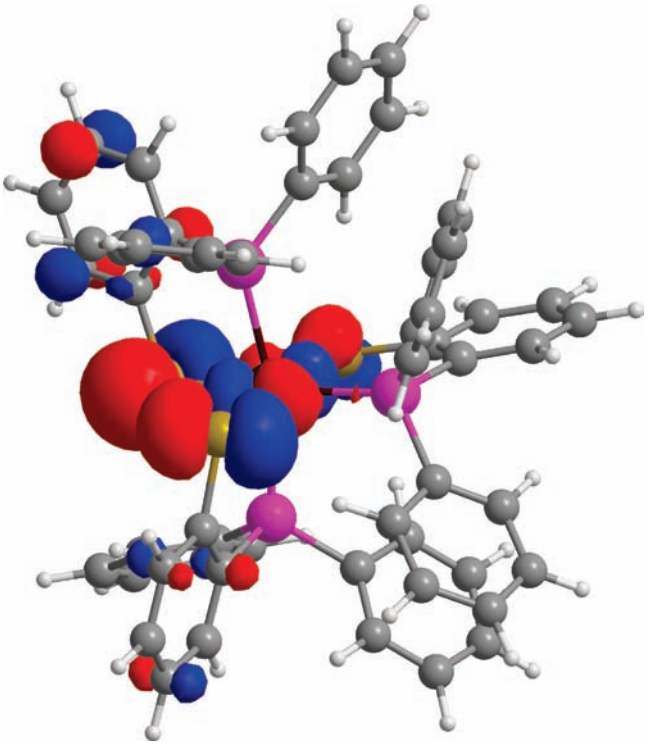

Figure 2. SOMO of **Ru-1** showing significant contributions from the Ru d_{xz} orbital and the in-phase p orbitals on S2 and S3.

O_2 sensitivity of [HNEt$_3$][**Ru-1**], which was noted to undergo one-electron metal-centered oxidation to **Ru-1** in dichloromethane and a six-electron sulfur-centered oxygenation to the sulfenato(RSO$^-$)/sulfinato(RSO$_2^-$) derivative in toluene, dichloromethane, and methanol mixtures.[36] We then synthesized [PPN][**Ru-1**] (PPN = bis(triphenylphosphoranylidene)-ammonium), which has improved solubility in organic solvents, to further investigate its oxidation chemistry.[37]

dx.doi.org/10.1021/ic200416y |*Inorg. Chem.* 2011, 50, 9904–9914

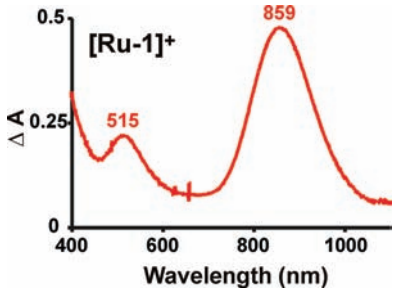

Figure 3. Absorbance spectrum of $[\mathbf{Ru\text{-}1}]^{+}$ calculated by subtracting one-half of the absorbance spectrum of **Ru-1** prior to oxidation by bulk electrolysis from a spectrum collected *in situ* during the oxidation after one-half of the calculated charge had been released; $\Delta A = A_{\text{half-ox.}} - 0.5A_{\text{initial}}$. A UV−visible trace of the oxidation recorded every 0.1 electron equivalents has been previously reported.[37]

As shown in Scheme 3, [PPN][**Ru-1**] displays a variety of metal- and ligand-centered reactions including alkylation,[38] oxidation,[37,39] and oxygenation.[40] The Ru(II) complex $[\mathbf{Ru\text{-}1}]^{-}$ can be oxidized in two successive one-electron steps to the formally Ru(III) and Ru(IV) derivatives **Ru-1** and $[\mathbf{Ru\text{-}1}]^{+}$. The half-potentials for these events versus ferrocenium/ferrocene are −830 mV and −20 mV for the $[\mathbf{Ru\text{-}1}]^{-/0}$ and $[\mathbf{Ru\text{-}1}]^{0/+}$ couples, respectively. Sulfur-centered alkylation of $[\mathbf{Ru\text{-}1}]^{-}$ in dichloromethane at room temperature yields the dithioether complex $[\mathbf{Ru\text{-}1}\cdot\mathbf{CH_2}]^{+}$, consistent with a high degree of metal−sulfur interaction in the frontier molecular orbitals. This suggests that oxidation of $[\mathbf{Ru\text{-}1}]^{-}$ may involve both the metal and sulfur.

The **Ru-1** derivative can be isolated by chemical oxidation via I_2 or by electrochemical methods.[37] The absorbance spectrum displays low-energy bands at 540 (ε = 1090), 797 (ε = 200), and 1041 (ε = 3020) nm, consistent with previously reported metal-coordinated thiyl radical complexes.[14,20] The formal oxidation state assignment of Ru(III) is further challenged by calculated Mulliken atomic spin densities of 0.62 on Ru and 0.20 and 0.17 on the thiolate donors S2 and S3, respectively.[39] Orbital analysis of the singly occupied molecular orbital (SOMO) of **Ru-1** reveals significant contributions from the d_{xz} orbital on Ru and the coplanar, in-phase S2-p_z and S3-p_x orbitals, Figure 2. The nearly equal metal and sulfur contributions to the SOMO combined with the approximately 60:40 distribution of spin density between Ru and the S donors is consistent with the assignment of **Ru-1** as a metal-stabilized thiyl radical.

Further oxidation of **Ru-1** has been investigated using chemical and electrochemical methods. The addition of O_2 to **Ru-1** or $[\mathbf{Ru\text{-}1}]^{-}$ results in irreversible sulfur-centered oxygenation.[40] The only detectable product after 24 h is the bis(sulfinato)-Ru(II) product, $[\mathbf{Ru\text{-}1}\cdot\mathbf{O_4}]^{-}$. The isolation of an anionic Ru(II) product from the neutral **Ru-1** requires reduction along with sulfur oxygenation. Through control reactions, we have shown hydroxide to be a competent reductant of the Ru^{III} sulfur−oxygenate $[\mathbf{Ru\text{-}1}\cdot\mathbf{O_4}]$ in acetonitrile. Further oxidations of **Ru-1** were conducted under anaerobic conditions.

The one-electron oxidation of **Ru-1** by electrochemical methods is reversible, as determined by cyclic voltammetry (CV) with a $[\mathbf{Ru\text{-}1}]^{+/0}$ redox couple of −20 mV.[37] Bulk oxidation of **Ru-1** reveals an EC process with an irreversible chemical step (C) that follows the reversible oxidation (E). A UV−visible trace recorded during the bulk oxidation of **Ru-1** in acetonitrile at

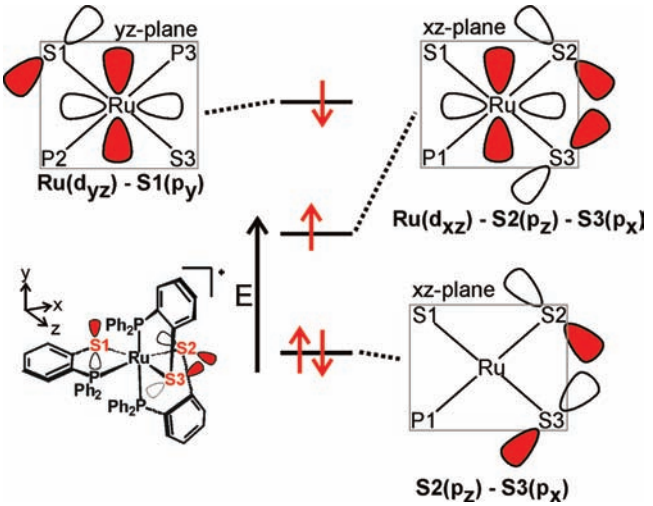

Figure 4. Qualitative overview of the frontier molecular orbitals of $[\mathbf{Ru\text{-}1}]^{+}$ determined by density functional theory calculations.[39] The highest singly occupied molecular orbital (SOMO) is nearly orthogonal to the SOMO−1 and highest fully occupied molecular orbital (HOMO), which are coplanar. The orientation of the sulfur p-type lone pairs perpendicular to the respective PS chelate plane are shown along with the assigned coordinate system in the lower left corner.

Scheme 4. Addition of Alkenes and Methyl Ketones to $[\mathbf{Ru\text{-}1}]^{+}$

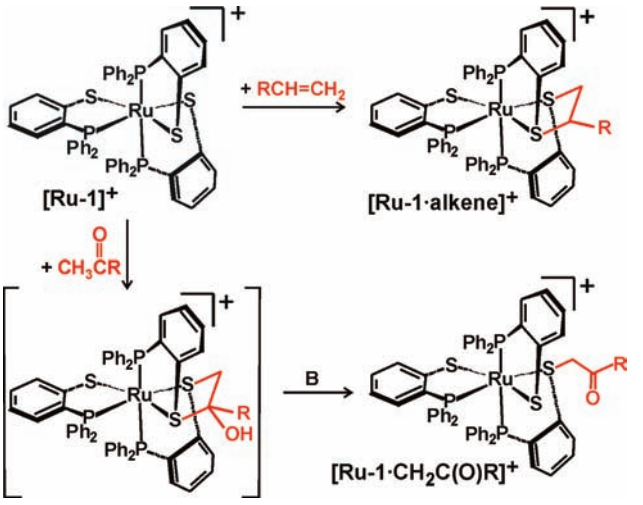

−20 °C reveals an intermediate with an absorbance band at 859 nm, Figure 3, assigned as $[\mathbf{Ru\text{-}1}]^{+}$, as supported by time-dependent density functional theory.[39] The low-energy band initially grows in intensity but then decays prior to completion of the one-electron oxidation. The final oxidation product is assigned as a Ru(II) complex with an intramolecular disulfide bond.

Density functional theory investigations of $[\mathbf{Ru\text{-}1}]^{+}$ reveal a nearly degenerate electronic ground state that is best described as a singlet diradical.[39] Significant spin localization is observed on Ru (0.84), S1 (0.31), S2 (0.47), and S3 (0.21). A qualitative overview of the frontier molecular orbitals, Figure 4, highlights the π interactions between Ru d orbitals and S p orbitals in the *xz*, *yz*, and *xy* planes. The configuration of the ground state is best described as $(S2(p_z) - S3(p_x))^2(d_{xz} - S2(p_z) - S3(p_x))^1(d_{yz} - S1(p_y))^1$.

dx.doi.org/10.1021/ic200416y |*Inorg. Chem.* 2011, 50, 9904–9914

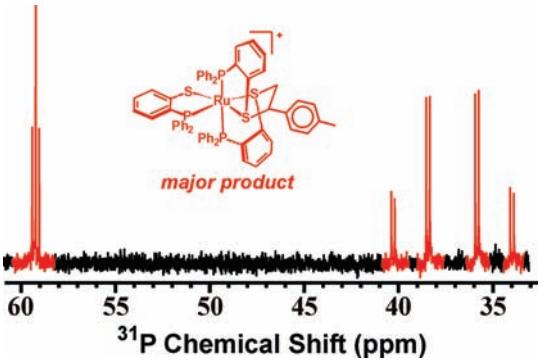

Figure 5. The ^{31}P NMR spectrum of crystalline [**Ru-1**·*p*-**methylstyrene**]$^{+}$ in CD_3CN. The spectrum matches the major product of the as-isolated mixture. Chemical shifts and coupling constants are provided in the text.

The diradical ground state of [**Ru-1**]$^{+}$ delocalizes the unpaired electrons of the metal-stabilized thiyl radicals over the metal and sulfur donors in nearly orthogonal molecular orbitals. This inhibits disulfide formation. In the absence of additional substrates, the rate constant for the decay of [**Ru-1**]$^{+}$ is 0.0101(6) s^{-1} at 272 K.[37] The relatively slow degradation of [**Ru-1**]$^{+}$ coupled with its significant sulfur-centered spin density make it a prime candidate for reactivity studies with unsaturated organic compounds.

IRREVERSIBLE ALKENE ADDITION

The oxidized intermediate [**Ru-1**]$^{+}$ reacts with alkenes and methyl ketones to yield dithioether alkene addition products, [**Ru-1**·**alkene**]$^{+}$, and monothioether ketone addition products, [**Ru-1**·$CH_2C(O)R$]$^{+}$, respectively, as shown in Scheme 4.[39,41,42] Through a series of bulk electrolysis experiments on freshly prepared solutions of **Ru-1**, we established the addition of alkenes to [**Ru-1**]$^{+}$ via a one-electron EC mechanism. In the electrochemical step, **Ru-1** is oxidized to [**Ru-1**]$^{+}$. The addition of the alkene in the following chemical step proceeds too rapidly to detect [**Ru-1**]$^{+}$ with UV−visible spectroscopy.

The ethylene addition product displays a [**Ru-1**·C_2H_4]$^{2+/+}$ redox couple at +285 mV assigned to the formal oxidation of Ru(II) to Ru(III).[41] A comparison of square voltammograms recorded before and after oxidation reveals quantitative conversion of [**Ru-1**·C_2H_4]$^{+}$ to [**Ru-1**·C_2H_4]$^{2+}$. The other alkene products display similar potentials for the $Ru^{III/II}$ redox couple. A potential of +280 mV is also observed for the [**Ru-1**·CH_2]$^{2+/+}$ couple of the methylene bridged complex isolated from the alkylation of [**Ru-1**]$^{-}$ with dichloromethane.[38] The large shift, +1110 mV, in the formal $Ru^{III/II}$ couple as compared to [**Ru-1**]$^{-/0}$ is consistent with the conversion of two thiolate donors to thioethers.[23,43,44]

The alkene addition product [**Ru-1**·**alkene**]$^{+}$ is air and water stable. There is no observed release of ethylene from [**Ru-1**·C_2H_4]$^{+}$ after prolonged purging with inert gases or overnight exposure to vacuum conditions. The stability of these complex is attributed to the favorable low-spin, d^6 electron configuration of Ru(II) in a phosphine and thioether donor environment.

The reaction with ketones proceeds more slowly via a two-electron ECE pathway.[42] The first electrochemical step generates [**Ru-1**]$^{+}$ with the expected low energy band at 859 nm in the absorbance spectrum. The addition of the ketone in the chemical step is proposed to proceed through the enol tautomer with rearrangement of the addition product to [**Ru-1**·$CH_2C(O)R$]$^{+}$. Since the [**Ru-1**·$CH_2C(O)R$]$^{2+/+}$ redox couple, −60 mV, is slightly more accessible than the [**Ru-1**]$^{+/0}$ couple, −20 mV, the second oxidation proceeds at the applied potential. As with the alkenes, the addition of methyl ketones to [**Ru-1**]$^{+}$ is irreversible.

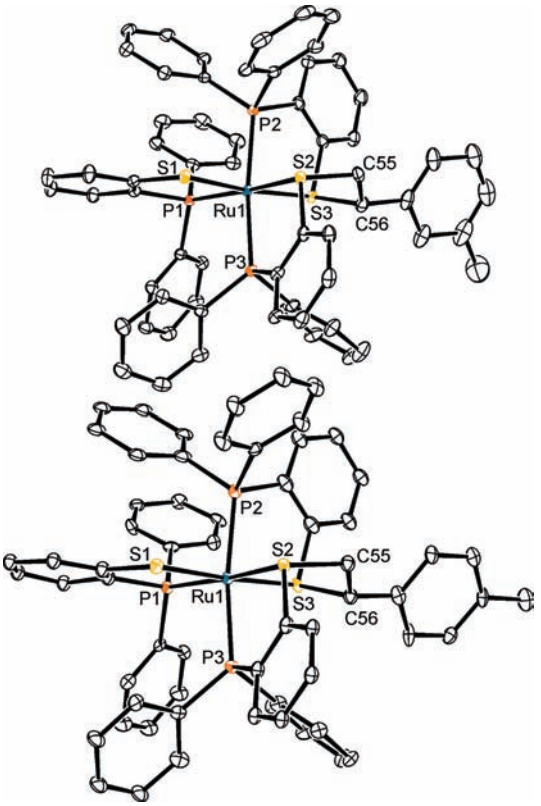

Figure 6. ORTEP representations of the complex cations of [**Ru-1**·*m*-**methylstyrene**][PF_6] (top) and [**Ru-1**·*p*-**methylstyrene**][PF_6] (bottom). Selected bond distances and angles are provided in Table 2.

The synthesis of [**Ru-1**·**alkene**]$^{+}$ derivatives by chemical oxidation has not been previously reported. It can be readily achieved upon the addition of mild chemical oxidants to [**Ru-1**]$^{-}$ in the presence of the appropriate alkenes. To demonstrate this reaction, we have prepared and isolated [**Ru-1**•*m*-**methylstyrene**]$^{+}$ and [**Ru-1**·*p*-**methylstyrene**]$^{+}$ as described in the Experimental Section. The complexes are obtained in 80% yield from [**Ru-1**]$^{-}$, two equivalents of $FcPF_6$, and the respective alkene. Analysis of the crude products by +ESI-MS reveals a single peak with m/z = 1099.20, consistent with the expected ratio of 1099.15. Alkene addition is confirmed through the observation of a single redox event at +224 and +284 mV for [**Ru-1**·*m*-**methylstyrene**]$^{+}$ and [**Ru-1**·*p*-**methylstyrene**]$^{+}$, respectively. The $Ru^{III/II}$ couples are shifted by approximately +1100 mV with respect to [**Ru-1**]$^{0/-}$.

Although the mass spectrum and cyclic voltammograms of [**Ru-1**·*p*-**methylstyrene**]$^{+}$ are consistent with a single product, the ^{31}P NMR spectrum of the "as isolated" compound reveals two reaction products with distinct spectra, Figure S1 (Supporting Information). The chemical shifts are temperature-independent, ruling out interconverting configurational isomers. Instead, the peaks are assigned to a pair of structural isomers that differ by the relative position of the aromatic

dx.doi.org/10.1021/ic200416y |*Inorg. Chem.* 2011, 50, 9904–9914

Table 1. Crystal Data and Structure Refinement for [Ru-1·*m*-methylstyrene][PF_6] and [Ru-1·*p*-methylstyrene][PF_6]

identification code	[Ru-1·*m*-methylstyrene][PF_6]	[Ru-1·*p*-methylstyrene][PF_6]
empirical formula	$C_{64.5}H_{52}Cl_3F_6P_4RuS_3$	$C_{75}H_{62}Cl_2F_6P_4RuS_3$
formula weight	1368.54	1469.29
temperature (K)	100(2)	100(2)
wavelength (Å)	0.71073	0.71073
crystal system	monoclinic	triclinic
space group	$P2_1$	$P1$
unit cell dimensions		
a (Å)	10.5855(4)	10.5684(8)
b (Å)	16.8551(5)	12.4018(9)
c (Å)	17.7704(4)	12.9434(6)
α (deg)	90	88.536(5)
β (deg)	104.576(3)	85.552(5)
γ (deg)	90	74.111(6)
vol (Å^3)	3068.53(18)	1626.71
Z	2	1
d_{calcd} (Mg/m^3)	1.481	1.500 Mg/m^3
abs coeff (mm^{-1})	0.651	0.580 mm^{-1}
F(000)	1392	752
cryst size (mm^3)	0.31 × 0.14 × 0.10	0.14 × 0.11 × 0.02 mm^3
θ range for data collection (deg)	3.38 to 29.65	3.30 to 28.14°
index ranges	$-14 \le h \le 13$	$-13 \le h \le 14$
	$-23 \le k \le 23$	$-15 \le k \le 16$
	$-24 \le l \le 22$	$-15 \le l \le 17$
reflns collected	50963	17453
independent refections	15701 [R(int) = 0.0498]	11533[R(int) = 0.0610]
completeness to theta max	94.5%	87.7%
absorption correction	SCALE3 ABSPACK	SCALE3 ABSPACK
max. and min transmission	0.952 and 0.926	0.996 and 0.931
refinement method	full-matrix least-squares on F^2	full-matrix least-squares on F^2
data/restraints/params	15701/27/778	11553/3/530
goodness of fit on F^2	1.014	1.09
final R indices [$I > 2\sigma(I)$][a,b]	R1 = 0.0438, wR2 = 0.1042	R1 = 0.0807, wR2 = 0.1399
R indices (all data)[a,b]	R1 = 0.0563, wR2 = 0.1136	R1 = 0.1109, wR2 = 0.1536
largest diff. peak and hole (e·Å^{-3})	1.372 and −0.564	1.660 and −0.955

[a] $R1 = \Sigma||F_o| - |F_c||/\Sigma|F_o|$. [b] $wR2 = \{\Sigma[w(F_o^2 - F_c^2)^2]/\Sigma[w(F_o^2)^2]\}^{1\backslash 2}$, where $w = q/\sigma^2(F_o^2) + (qp)^2 + bp$. GOF = $S = \{\Sigma[w(F_o^2 - F_c^2)^2]/(n-p)\}^{1/2}$, where n is the number of reflections and p is the number of parameters refined.

substituent in the addition product. The major component (65%) displays a second-order spectrum with chemical shifts (ppm) of $\delta_1 = 59.2$, $\delta_2 = 39.2$, and $\delta_3 = 35.1$ and coupling constants (Hz) of $J_{12} = J_{13} = 30$ and $J_{23} = 300$. The chemical shifts and coupling constants are similar to those of previously reported related complexes.[36,38,41,45] A similar second-order spectrum is observed for the minor component (35%); $\delta_1 = 54.7$, $\delta_2 = 44.4$, $\delta_3 = 35.9$ ppm, $J_{12} = J_{13} = 28$, and $J_{23} = 316$ Hz. Crystallization of [**Ru-1·*p*-methylstyrene**]$^+$ yields yellow plates, which display a ^{31}P NMR spectrum consistent with the major isomer, Figure 5. Repeated attempts to crystallize the minor component have been unsuccessful. The [**Ru-1·*m*-methylstyrene**]$^+$ products are similar, with $\delta_1 = 59.3$, $\delta_2 = 39.1$, and $\delta_3 = 35.2$ ppm and $J_{12} = J_{13} = 30$ and $J_{23} = 300$ Hz for the major isomer and $\delta_1 = 54.8$, $\delta_2 = 44.3$, and $\delta_3 = 35.9$ ppm and $J_{12} = J_{13} = 32$ and $J_{23} = 318$ Hz for the minor.

X-ray-quality yellow plate crystals of [**Ru-1·*p*-methylstyrene**][PF_6] and [**Ru-1·*m*-methylstyrene**][PF_6] were obtained through the evaporation of concentrated chlorobenzene or 1:1 dichloromethane/hexane solutions. ORTEP[46] representations of the cationic complexes are shown in Figure 6. Details of the data collection and refinement are summarized in Table 1. In each instance, the complex maintains a meridional M(PS)$_3$ core structure with the addition of the alkene across S2 and S3, similar to [**Ru-1·C_2H_4**]$^+$.[41] To date, only one isomer of each complex has been crystallized. In both cases, the X-ray structure reveals the unsubstituted carbon, C55, bonded with S2, which is the sulfur trans to P1. As shown in Table 2, there are no significant differences in the primary coordination sphere of the three complexes. Alkene coordination generates a five-member Ru(1)−S(2)−C(55)−C(56)−S(3) puckered ring. The average S(2)−C(55) and S(3)−C(56) bond distances of 1.83(2) and 1.86(2) Å are consistent with single bond formation between the coordinated sulfur and the alkene. Also, the average and C(55)−C(56) bond distance of 1.50(2) Å confirms single bond character and covalent coordination of the alkene to the metal-stabilized thiyl radical precursor.

dx.doi.org/10.1021/ic200416y |*Inorg. Chem.* 2011, 50, 9904–9914

Table 2. Selected Bond Distances (Å) and Bond Angles (deg) for $[\text{Ru-1}\cdot C_2H_4]^+$,[41] $[\text{Ru-1}\cdot m\text{-methylstyrene}]^+$, and $[\text{Ru-1}\cdot p\text{-methylstyrene}]^+$

	$[\text{Ru-1}\cdot C_2H_4]^+$	$[\text{Ru-1}\cdot m\text{-methylstyrene}]^+$	$[\text{Ru-1}\cdot p\text{-methylstyrene}]^+$
Ru−S1	2.3856(9)	2.3735(9)	2.389(3)
Ru−S2	2.3749(9)	2.3707(9)	2.373(3)
Ru−S3	2.3365(9)	2.3404(9)	2.320(2)
Ru−P1	2.3290(9)	2.3423(9)	2.333(3)
Ru−P2	2.3965(10)	2.3623(9)	2.350(3)
Ru−P3	2.3648(9)	2.3717(9)	2.391(3)
S2−C55	1.836(4)	1.818(4)	1.838(9)
S3−C56	1.843(4)	1.883(4)	1.867(10)
C55−C56	1.510(5)	1.501(6)	1.483(13)
S2−Ru−S3	87.71(3)	87.86(3)	87.67(9)
P2−Ru−P3	168.81(3)	170.64(3)	169.64(10)
S1−Ru−S2	87.06(3)	85.81(3)	87.14(9)
S1−Ru−S3	173.73(3)	172.50(3)	174.37(11)
S2−C55−C56	114.0(3)	114.1(3)	113.8(7)
S3−C56−C55	112.8(3)	112.0(3)	110.1(7)

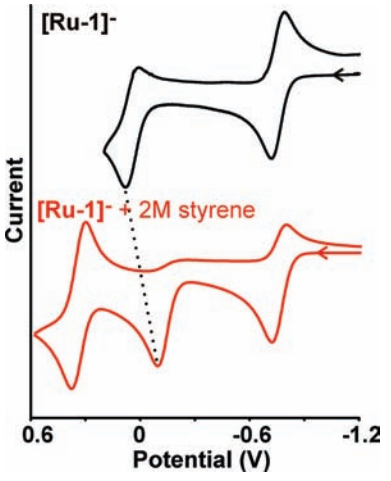

Figure 7. Cyclic voltammograms of $[\text{Ru-1}]^-$ in the absence (top) and presence (bottom) of 2 M styrene. Data were collected in acetonitrile with 0.1 M tetrabutylammonium hexafluorophosphate as a supporting electrolyte. Potentials are referenced versus Fc^+/Fc.

In the crystal structures of both $[\text{Ru-1}\cdot m\text{-methylstyrene}]^+$ and $[\text{Ru-1}\cdot p\text{-methylstyrene}]^+$, the unsubstituted carbon of the styrene is bonded to S2 and the sulfur trans to P1. The S2 and S3 sites can also be differentiated by their calculated spin density, which is more than twice as high on S2 (0.47) than on S3 (0.21). Since Tedder's Rules[47] for radical alkene addition suggest that substitution should occur initially at the nonsubstituted carbon, we tentatively assign the crystal structures of $[\text{Ru-1}\cdot m\text{-methylstyrene}]^+$ and $[\text{Ru-1}\cdot p\text{-methylstyrene}]^+$ to the major products observed in the ^{31}P NMR.

To obtain further insight into the alkene addition mechanism, CV was used to determine rate constants for the addition of various alkenes to the oxidized intermediate $[\text{Ru-1}]^+$. The rapid addition of alkenes to $[\text{Ru-1}]^+$ results in significant changes in the cyclic voltammograms of $[\text{Ru-1}]^-$, Figure 7, that can be simulated according to an EECE mechanism, Scheme 5. The first two electrochemical steps are assigned to the oxidation of $[\text{Ru-1}]^-$ to $[\text{Ru-1}]^+$ in successive one-electron steps. The cathodic return peak currents associated with these events are greatly diminished due to the irreversible formation of $[\text{Ru-1}\cdot\text{alkene}]^n$ during oxidation. The rapid alkene addition to $[\text{Ru-1}]^+$ in the chemical step disrupts the equilibrium concentrations of $[\text{Ru-1}]^{+/0}$ and shifts the apparent anodic potential to lower potentials. The final electrochemical step is the oxidation of the alkene addition

Scheme 5. EECE Mechanism for the Addition of Alkenes to $[\text{Ru-1}]^-$

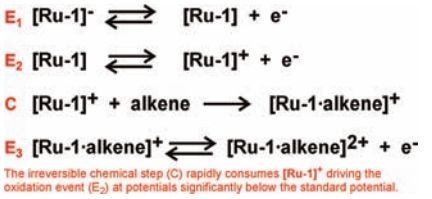

Table 3. Second-Order Rate Constants for the Addition of Selected Alkenes to $[\text{Ru-1}]^+$ in Acetonitrile at 298 K[a]

alkene	k (M^{-1} s^{-1})
monosubstituted alkenes	
styrene	$4.6(5) \times 10^7$
n-propyl vinyl ether	$2.0(1) \times 10^7$
t-butyl vinyl ether	$2.6(8) \times 10^6$
n-hexene	$7(2) \times 10^5$
acrylonitrile	$2.7(2) \times 10^4$
cyclic alkenes	
norborene	$4(2) \times 10^7$
cyclopentene	$6(1) \times 10^6$
cyclohexene	$2.9(3) \times 10^3$

[a] Rate constants were determined by simulation of cyclic voltammetry data collected at multiple scan rates, as described in the Supporting Information.

dx.doi.org/10.1021/ic200416y |*Inorg. Chem.* 2011, 50, 9904–9914

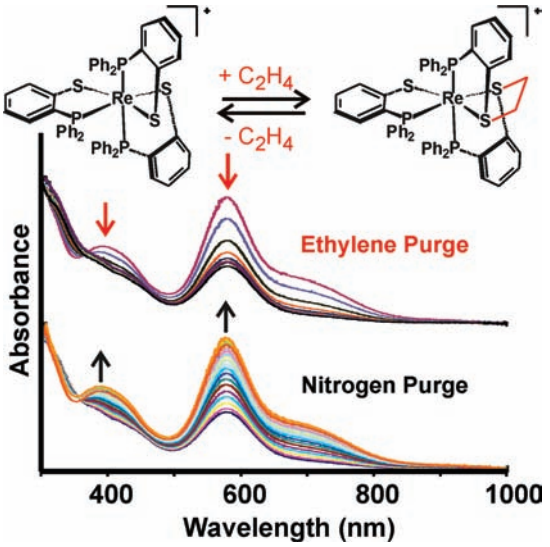

Figure 8. Absorbance spectra showing the reversible binding of ethylene to $[\mathbf{Re\text{-}1}]^+$. The absorbance bands at 390 and 581 nm decrease in intensity upon the introduction of ethylene gas (top) until the bands reach ~46% of their initial intensity. The bands are restored by purging the solution with nitrogen. Spectra were recorded every 30 s.

product by one electron from $[\mathbf{Ru\text{-}1 \cdot alkene}]^+$ to $[\mathbf{Ru\text{-}1 \cdot alkene}]^{2+}$. As described in the Supporting Information, rate constant data were extracted for a variety of alkenes using the DigiSim software package.[48]

Experimentally determined rate constants for the addition of various alkenes to $[\mathbf{Ru\text{-}1}]^+$ are summarized in Table 3. The data are consistent with an electrophilic metal-stabilized thiyl radical. The nonfunctionalized alkene, 1-hexene, displays a second-order rate constant of $7(2) \times 10^5\ M^{-1}\ s^{-1}$. The "electron-rich" alkenes styrene, *n*-propyl vinyl ether, and *t*-butyl vinyl ether add more rapidly, while the "electron-poor" acrylonitrile displays a reduced rate constant. Similar observations for the addition of haloalkyl[49] and *t*-butoxy radicals[50] to alkenes were reported by Hosomi et al. and Solomon et al., respectively. For cyclic alkenes, the rate constant is related to the amount of ring strain in the alkene precursor; $k_{norborene} > k_{cyclopentene} > k_{cylcohexene}$.

Overall, a variety of alkenes can be added to $[\mathbf{Ru\text{-}1}]$ upon oxidation to yield the corresponding dithioether−Ru(II) derivatives. The addition proceeds via an electrophilic ruthenium-stabilized thiyl radical, $[\mathbf{Ru\text{-}1}]^+$, with the fastest rate constants observed for "electron-rich" alkenes and cyclic alkenes with significant ring strain. In all cases, the addition is *irreversible*. The insurmountable barrier to C−S bond cleavage can be attributed to the thermodynamic stability of the dithioether−Ru(II) products. As such, we sought other derivatives that would prove more amenable to C−S bond cleavage and reversible alkene binding.

REVERSIBLE ALKENE ADDITION

Although our results with $[\mathbf{Ru\text{-}1}]^+$ demonstrated facile C−S bond formation with alkenes to generate the desired $[\mathbf{Ru\text{-}1 \cdot alkene}]^+$, the thermodynamic stability of the product precluded reversibility. Reports of C−S bond cleavage with release of ethylene upon reduction of the Re(II) complex $[Re(TTCN)]^{2+}$ (TTCN = 1,4,7-trithiacyclononane) by Went et al. provided a lead.[51] Computational studies by Rothlisberger et al.

Scheme 6. Thermodynamic Squares for $[\mathbf{Re\text{-}1}]^n$ and $[\mathbf{Re\text{-}1 \cdot C_2H_4}]^n$ (n = 0, +1, +2)

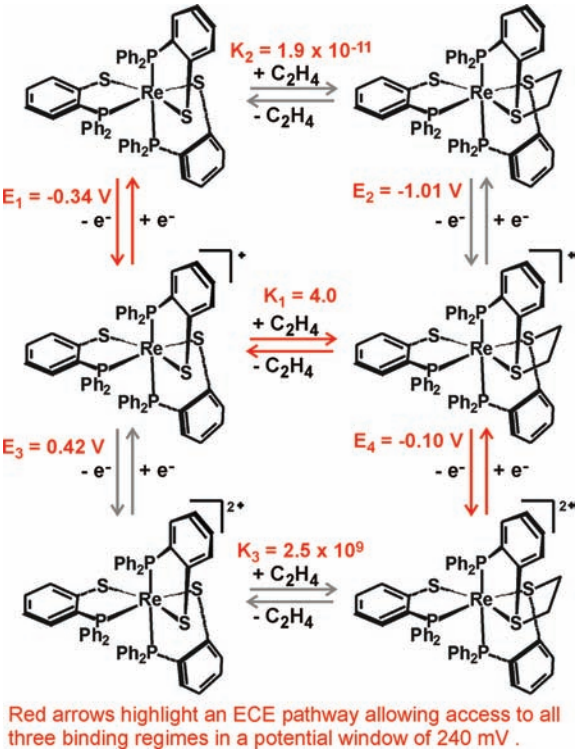

on the release of ethylene from $[Re(TTCN)]^{2+}$ confirmed a drop in the energy barrier for C−S bond cleavage from 22 to 4 kcal/mol upon reduction.[52,53] This 18 kcal/mol decrease in activation energy was attributed to a combination of charge and π-back-bonding effects. Related studies on the $[Ru(TTCN)]^{2+}$ derivative predict an activation energy for ethylene release of 44 kcal/mol, consistent with the observed stability of our Ru(II) $[\mathbf{Ru\text{-}1 \cdot alkene}]^+$ complexes. As such, to achieve *reversible* alkene binding, we turned our attention to the rhenium derivative, **Re-1**.

Unlike **Ru-1**, solutions of **Re-1** are stable in the air and show no detectable reaction with dichloromethane after one week. The neutral complex displays two reversible oxidation events at −340 and +420 mV assigned to the $[\mathbf{Re\text{-}1}]^{+/0}$ and $[\mathbf{Re\text{-}1}]^{2+/+}$ redox couples, respectively.[35,54] A $[\mathbf{Re\text{-}1}]^{0/-}$ reduction event is also observed at −1620 mV. Although **Re-1** has the same valence electron count as $[\mathbf{Ru\text{-}1}]^+$, the neutral precursor does not react with ethylene. This is attributable to the difference in charge of the two complexes, which was predicted by Rothlisberger to significantly influence the energy barrier for C−S bond cleavage.[52]

Oxidation of **Re-1** to $[\mathbf{Re\text{-}1}]^+$ by chemical or electrochemical methods yields a deep blue solution that reversibly binds ethylene.[54] As shown in Figure 8, the absorbance band at 581 nm decreases to 45% of its initial intensity within 150 s. No further changes in the absorbance band are noted at longer reaction times, indicating the process is in dynamic equilibrium with an equilibrium binding constant of approximately $2.6\ M^{-1}$. Purging the solution with nitrogen restores the initial intensity of the 581 nm band within 300 s. The process can be repeated multiple times with no detectable loss of binding/release efficiency.

To refine the ethylene binding constant and establish rate constants for ethylene binding/release, cyclic voltammograms of

dx.doi.org/10.1021/ic200416y |*Inorg. Chem.* 2011, 50, 9904–9914

$[\mathbf{Re\text{-}1}]^+$ were recorded under nitrogen and ethylene atmospheres.[54] Simulation of the data over a range of scan rates from 100 to 1000 mV/s revealed rate constants for ethylene addition and release of 0.12(2) M^{-1} s^{-1} and 0.030(4) s^{-1}, respectively. The equilibrium binding constant of 4.0(8) M^{-1} matches the prediction from the UV−visible study.

Using the experimentally determined redox potentials for $[\mathbf{Re\text{-}1}]^n$ and $[\mathbf{Re\text{-}1}\cdot\mathbf{C_2H_4}]^n$ with the equilibrium binding constant for ethylene to $[\mathbf{Re\text{-}1}]^+$, we constructed the set of thermodynamic boxes, Scheme 6.[54] From these, we determined equilibrium binding constants for ethylene to the neutral **Re-1** complex, 1.9(4) × 10^{-11} M^{-1}, and the dicationic $[\mathbf{Re\text{-}1}]^{2+}$, 2.5(9) × 10^9 M^{-1}. As highlighted by following an ECE path through Scheme 6 from **Re-1** to $[\mathbf{Re\text{-}1}\cdot\mathbf{C_2H_4}]^{2+}$, the three distinct ethylene binding regimes are accessible and only separated by 240 mV. Mild oxidants can be employed with **Re-1** to induce strong ethylene binding, while mild reductants can induce its release from $[\mathbf{Re\text{-}1}\cdot\mathbf{C_2H_4}]^{2+}$. Using this approach, we have isolated $[\mathbf{Re\text{-}1}\cdot\mathbf{C_2H_4}]^{2+}$ through the chemical oxidation of $[\mathbf{Re\text{-}1}]$ with $AgPF_6$ in an ethylene saturated solution.

Attempts to measure rate constants for the addition of various alkenes to $[\mathbf{Re\text{-}1}]^+$ by CV following the protocol established for $[\mathbf{Ru\text{-}1}]^+$ were unsuccessful. Chemical oxidation of $[\mathbf{Re\text{-}1}]^+$ by $AgPF_6$ in the presence of styrene confirms the formation of $[\mathbf{Re\text{-}1}\cdot\mathbf{styrene}]^+$, but with a rate constant it is too slow to detect on the time scale of the CV experiments. Preliminary UV−visible studies suggest a rate constant on the order of 10^{-5} M^{-1} s^{-1}, which is below our CV detection limit of 1 × 10^{-3} M^{-1} s^{-1}.

The rate constant for styrene addition to $[\mathbf{Re\text{-}1}]^+$ is 4 orders of magnitude slower than that of ethylene, indicating that $[\mathbf{Re\text{-}1}]^+$ can selectively bind ethylene even in the presence of other alkenes. Further, the rate constant for styrene addition to $[\mathbf{Re\text{-}1}]^+$ is 12 orders of magnitude slower than that to $[\mathbf{Ru\text{-}1}]^+$. This would be consistent with a linear free energy relationship between the rate constant and equilibrium binding constant with fast irreversible addition of alkenes to $[\mathbf{Ru\text{-}1}]^+$ and slow, reversible addition to $[\mathbf{Re\text{-}1}]^+$.

CONCLUDING REMARKS

The addition of alkenes to the oxidized metal−thiolate complexes $[\mathbf{Ru\text{-}1}]^+$ and $[\mathbf{Re\text{-}1}]^+$ is consistent with their assignments as metal-stabilized thiyl radicals. The addition occurs selectively across the S2/S3 sulfur pair, which is differentiated from S1 by the directionality of their p-type "lone pair" orbitals, as shown in Figure 4. The in-phase combination of the S2/S3 p-type orbitals interacts in an antibonding capacity with the metal d_{yz} orbital generating a half-occupied, frontier molecular orbital. As shown in Figure 4, this orbital has the proper symmetry to interact with the HOMO of the approaching alkene.

Alkene addition to our metal-stabilized thiyl radicals initiates a net two-electron transfer from the alkene to the metal-stabilized thiyl radical complex, resulting in a two-electron reduction in the *formal* oxidation state of the metal ion. For $[\mathbf{Ru\text{-}1}]^+$, the *formal* Ru^{IV} is readily reduced to Ru^{II} in the thermodynamically stable $[\mathbf{Ru\text{-}1}\cdot\mathbf{alkene}]^+$ product. Although our computational studies also find the requisite half-occupied frontier molecular in the *neutral* **Ru-1** complex, alkene addition does not occur, as the putative Ru(I) product, **Ru-1·alkene**, is thermodynamically unfavorable. As such, reduction of $[\mathbf{Ru\text{-}1}\cdot\mathbf{alkene}]^+$ to **Ru-1·alkene** would be expected to initiate the C−S bond, but the $[\mathbf{Ru\text{-}1}\cdot\mathbf{alkene}]^{+/0}$ redox couple lies outside the solvent window of common organic solvents, making the addition of alkenes to $[\mathbf{Ru\text{-}1}]^+$ *irreversible.*

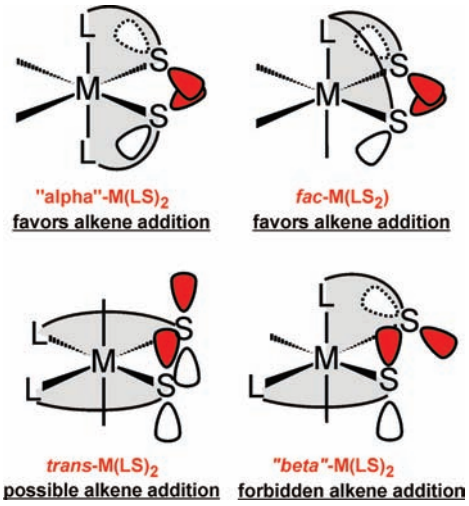

Figure 9. Orientation of thiolate lone pairs in various chelate geometries. The p-type lone pair on sulfur is placed orthogonal to the LS chelate plane (shaded). The predicted alkene reactivity is based on the symmetry of the thiolate lone pairs relative to the HOMO of an alkene, as described in the text.

If the only requirements for alkene addition to a metal-stabilized thiyl radical were the symmetry of the frontier molecular orbitals and the accessibility of a suitable oxidation state of the product, **Re-1** would be expected to display similar reactivity to $[\mathbf{Ru\text{-}1}]^+$. It does not. As described by Rothlisberger et al., the charge of the complex is also important. The low binding affinity of **Re-1** for ethylene is ascribed to the relatively high energy of the $\mathbf{Re\text{-}1}\cdot\mathbf{C_2H_4}$ and **Re-1** frontier orbitals with respect to the HOMO of ethylene. Oxidation of the Re complexes to their cationic derivatives lowers the energies of their molecular orbitals, providing a better energetic match with the HOMO of ethylene. For $[Re(TTCN)_2]^{3+/2+}$, a +1 change in charge was calculated to increase the energy barrier for ethylene release by 18 kcal/mol.[52] Similarly, in our system, oxidation of **Re-1** to $[\mathbf{Re\text{-}1}]^+$ stabilizes ethylene binding by 15.4 kcal/mol. Further oxidation of $[\mathbf{Re\text{-}1}]^+$ to $[\mathbf{Re\text{-}1}]^{2+}$ results in an additional 12.0 kcal/mol of stabilization.

With the insight gleamed from the $[\mathbf{Ru\text{-}1}]^n$ and $[\mathbf{Re\text{-}1}]^n$ systems, we can predict general features that would promote alkene addition to metal-stabilized thiyl radicals. To identify potential metal-stabilized thiyl radicals, the nucleophilic character of the coordinated thiolate can serve as a predictor of high metal−sulfur contributions in the frontier molecular orbitals. The ligand framework should be designed to provide a SOMO with the proper symmetry to matche the alkenes' HOMO. As shown in Figure 9, this can be accomplished with *cis*-dithiolate metal precursors with coplanar sulfur lone pairs dictated by chelation. In an octahedral environment, bis-chelates or tetradentate donors should adopt an "α-isomer" confirmation, while tridentate ligands should be facially coordinating to promote the interaction of the metal d orbital with coplanar sulfur p orbitals, as shown in Figure 4. A "trans-isomer" orientation has perpendicular sulfur lone pairs with an in-phase combination that can also overlap with the HOMO of an alkene. A potential drawback of this arrangement is the relative position of the symmetry preferred molecular orbital below the out-of-phase S−p combination.

dx.doi.org/10.1021/ic200416y |*Inorg. Chem.* 2011, 50, 9904–9914

Regarding oxidation and charge state preferences, alkene addition requires a net two-electron reduction of the metal-stabilized thiyl radical. The *formal* oxidation state of the reactive complex should be high enough to yield an accessible oxidation state in the alkene addition product. If the products' oxidation state is inaccessible, alkene addition will not occur. If the product will be generated in the lowest accessible oxidation state, addition will likely be irreversible. Finally, addition products with accessible redox couples can be reduced to lower alkene binding affinity and oxidized to enhance it. Future efforts to develop new complexes to demonstrate alkene binding to metal-stabilized thiyl radicals and the development of potential applications is underway.

EXPERIMENTAL SECTION

Materials and Methods. All chemicals were purchased from commercial sources (Aldrich) and used without further purification unless otherwise noted. All solvents were purified utilizing the standard methods and were freshly distilled and degassed using the freeze−pump−thaw method immediately before use. The metal−thiolate complexes **PPN[Ru-1]**,[37] **$HNEt_3$[Ru-1]**,[36] and **Re-1**[35] were synthesized according to published procedures. Deuterated acetonitrile was purchased from Cambridge Isotope Laboratories, Inc. and used as received. All reactions were conducted under anaerobic conditions by using standard Schlenk techniques under a nitrogen atmosphere.

[Ru-1·*m*-methylstyrene][PF_6]. To a yellow solution of **$HNEt_3$-[Ru-1]** (100 mg, 0.0935 mmol) in acetonitrile (40 mL) was added *m*-methylstyrene (0.0621 mL, 0.468 mmol) via syringe. The solution was cooled in an ice bath, and a blue solution of ferrocenium hexafluorophosphate (0.0619 g, 0.0187 mmol) in acetonitrile (30 mL) was added by cannula transfer. The resulting solution was stirred for 3 h, during which time the color changed to a yellow-green. The solvent was removed by rotary evaporation to yield a yellow residue. The crude product was washed with an excess of hot water (∼300 mL) and diethyl ether (25 mL). Yield: 0.090 g (82%). X-ray quality crystals were obtained by the addition of 30 mg of crude product to a mixture of dichloromethane (1 mL) and hexane (1 mL). Slow evaporation yielded yellow X-ray quality crystals. $E_{1/2}(Ru^{III}/Ru^{II})$ = +224 mV. +ESI-MS for $C_{63}H_{52}P_3S_3Ru$, theoretical: m/z (Z = 1) 1099.15. Observed: 1099.20. Element analysis for $C_{65}H_{56}P_4S_3F_6Ru$, calculated: C, 61.35; H, 4.44. Found: C, 61.50; H, 4.73.

[Ru-1·*p*-methylstyrene][PF_6]. The complex is prepared by the method described above except that *p*-methylstyrene (0.0618 mL, 0.468 mmol) was added in place of *m*-methylstyrene. Yield: 0.088 g (80%). X-ray quality yellow plate crystals were obtained from the evaporation of chlorobenzene solutions. $E_{1/2}(Ru^{III}/Ru^{II})$ = +284 mV. +ESI-MS for $C_{63}H_{52}P_3S_3Ru$, theoretical: m/z (Z = 1) 1099.15. Observed: 1099.20. Element analysis for $C_{65}H_{56}P_4S_3F_6Ru$, calculated: C, 61.35; H, 4.44. Found: C, 60.99; H, 4.73.

Physical Methods. NMR spectra were recorded on a Varian 400 MHz spectrometer and referenced to TMS (^{1}H NMR) and 85% H_3PO_4 (^{31}P NMR). Elemental analysis was performed by the Midwest Microlab (Indianapolis, IN). Mass spectra were collected by the Mass Spectrometry Application and Collaboration Facility in the Chemistry Department at Texas A&M University. All electrochemical measurements were performed by using a PAR 273 potentiostat/galvanostat with a three-electrode cell (glassy carbon working electrode, platinum wire counter electrode, and Ag/Ag ion reference electrode). Reported potentials are scaled versus a ferrocenium/ferrocene standard (0.00 V), which was determined using an internal standard. Full details regarding the determination of rate constants by cyclic voltammetry are provided in the Supporting Information.

Crystallographic Studies. A yellow needle 0.31 × 0.14 × 0.10 mm^3 crystal of [**Ru-1·*m*-methylstyrene**][PF_6] was mounted on a glass fiber for collection of X-ray data on an Agilent Technologies/Oxford Diffraction Gemini CCD diffractometer. The CrysAlisPro[55] CCD software package (v 171.33.34d) was used to acquire a total of 668 30-s frame ω-scan exposures of data at 100 K to a 2θ max = 59.30° using monochromated Mo Kα radiation (0.71073 Å) from a sealed tube. Frame data were processed using CrysAlisPro[55] RED to determine final unit cell parameters: a = 10.5855(4) Å, b = 16.8551(5) Å, c = 17.7704(4) Å, β = 104.576(3)°, V = 3068.53(18) Å^3, D_{calc} = 1.481 Mg/m^3, and Z = 2 to produce raw *hkl* data that were then corrected for absorption (transmission min./max. = 0.952/0.926; μ = 0.651 mm^{-1}) using SCALE3 ABSPACK in CrysAlisPro.[55] The structure was solved by Patterson methods in the space group $P2_1$ using SHELXS-90[56] and refined by least-squares methods on F^2 using SHELXL-97[57] incorporated into the SHELXTL[58] (v 6.14) suite of programs. Non-hydrogen atoms were refined with anisotropic atomic displacement parameters (except for the 20% occupancy F atoms, which were refined isotropically). The hexafluorophosphate anion has a tumbling disorder that was modeled with one 60% occupancy (F1a−F6a) group and two 20% occupancy (F1b−F6b and F1c−F6c) groups of fluorine atoms. The ratio for the anion disorder was fixed at 60:20:20 after being determined from unstable refinement of the F-atom occupancies. The disordered full occupancy methylene chloride solvate was modeled with two 50% occupancy groups, Cl1a−Cl2a and Cl1b−Cl2b, in addition to the full occupancy C atom. The 1/2 occupancy methylene chloride was modeled with two 25% occupancy groups, Cl3a−Cl4a and Cl3b−Cl4b, and a 50% C atom. Hydrogen atoms were placed in their geometrically generated positions and refined as a riding model. Methylene, methine, and phenyl H's were included as fixed contributions with U(H) = 1.2 × Ueq (attached C atom) while methyl groups were allowed to ride (the torsion angle which defines its orientation was allowed to refine) on the attached C atom, and these atoms were assigned U(H) = 1.5 × Ueq. For all 15 701 unique reflections (R(int) 0.049), the final anisotropic full matrix least-squares refinement on F^2 for 778 variables converged at R1 = 0.056 and wR2 = 0.113 with a GOF of 1.01.

After numerous attempts, crystals of [**Ru-1·*p*-methylstyrene**][PF_6] suitable for X-ray analysis were grown by slow evaporation of chlorobenzene solution and mounted on a CryoLoop for collection of X-ray data on an Agilent Technologies/Oxford Diffraction Gemini CCD diffractometer. X-ray structural analysis for [**Ru-1·*p*-methylstyrene**][PF_6] was performed on a 0.14 × 0.11 × 0.02 mm^3 yellow plate using a 463 frame, 55-s frame ω-scan data collection strategy at 100 K to a $2\theta_{max}$ = 56.30°. [**Ru-1·*p*-methylstyrene**][PF_6] crystallizes in the space group $P1$ with unit cell parameters a = 10.5684(8) Å, b = 12.4018(9) Å, c = 12.9434(6) Å, α = 88.536(5)°, β = 85.552(5)°, γ = 74.111(6)°, V = 1626.71(18) Å^3, Z = 1, and D_{calc} = 1.500 Mg/m^3. A total of 11 553 raw independent data were corrected for absorption (transmission min./max. = 0.996/0.931; μ = 0.580 mm^{-1}). The structure was solved by Patterson methods using SHELXTL[58] as well as by direct methods using SIR97[59] and charge-flipping using OLEX2.[22,23] All non-hydrogen atoms were refined with anisotropic atomic displacement parameters. Hydrogen atoms were included as fixed contributions, as described above for [**Ru-1·*m*-methylstyrene**][PF_6]. For reflections $I > 2\sigma(I)$ (R(int) 0.061), the final anisotropic full matrix least-squares refinement on F^2 for 530 variables converged at R1 = 0.080 and wR2 = 0.139 with a GOF of 1.09.

ASSOCIATED CONTENT

Supporting Information. Data fitting procedure for determination of alkene addition rate constants, best-fit CV parameters, ^{31}P NMR of [**Ru-1·*p*-methylstyrene**]$^+$ as-isolated showing major and minor products, and +ESI-MS for [**Ru-1·*m*-methylstyrene**]$^+$ and [**Ru-1·*p*-methylstyrene**]$^+$ in PDF

format and crystallographic data in CIF format (CCDC 814546 and 814547). This material is available free of charge via the Internet at http://pubs.acs.org.

AUTHOR INFORMATION

Corresponding Author
*E-mail: grapperhaus@louisville.edu.

ACKNOWLEDGMENT

C.A.G. expresses sincere gratitude to the students and collaborators who helped define and develop this project, especially Dr. Selma Poturovic and Kiran Venna. The authors thank Rajat Chauhan for assistance with NMR studies. We acknowledge the Donors of the American Chemical Society Petroleum Research Fund (43917-AC3) and the National Science Foundation (CHE-0238137) for financial support during the early stages of this project. M.S.M. thanks the Department of Energy, grant number DE-FG02-08CH11538, and the Kentucky Research Challenge Trust Fund for the upgrade of our X-ray facilities.

REFERENCES

(1) Benedito, F. v. L.; Petrenko, T.; Bill, E.; Weyhermüller, T; Wieghardt, K. *Inorg. Chem.* **2009**, *48*, 10913–10925.
(2) Le Goff, A.; Le Roy, C.; Pétillon, F. Y.; Schollhammer, P.; Talarmin, J. *Organometallics* **2007**, *26*, 3607–3610.
(3) Grapperhaus, C. A.; Darensbourg, M. Y. *Acc. Chem. Res.* **1998**, *31*, 451–459.
(4) O'Toole, M. G.; Kreso, M.; Kozlowski, P. M.; Mashuta, M. S.; Grapperhaus, C. A. *J. Biol. Inorg. Chem.* **2008**, *13*, 1219–1230.
(5) Masitas, C. A.; Mashuta, M. S.; Grapperhaus, C. A. *Inorg. Chem.* **2010**, *49*, 5344–5346.
(6) Masitas, C. A.; Kumar, M.; Mashuta, M. S.; Kozlowski, P. M.; Grapperhaus, C. A. *Inorg. Chem.* **2010**, *49*, 10875–10881.
(7) Jiang, Y. B.; Widger, L. R.; Kasper, G. D.; Siegler, M. A.; Goldberg, D. P. *J. Am. Chem. Soc.* **2010**, *132*, 12214–12215.
(8) Badiei, Y. M.; Siegler, M. A.; Goldberg, D. P. *J. Am. Chem. Soc.* **2011**, *133*, 1274–1277.
(9) Shearer, J.; Callan, P. E.; Amie, J. *Inorg. Chem.* **2010**, *49*, 9064–9077.
(10) Harrop, T. C.; Mascharak, P. K. *Acc. Chem. Res.* **2004**, *37*, 253–260.
(11) Kovacs, J. A. *Chem. Rev.* **2004**, *104*, 825–848.
(12) Arakawa, T.; Kawano, Y.; Katayama, Y.; Nakayama, H.; Dohmae, N.; Yohda, M.; Odaka, M. *J. Am. Chem. Soc.* **2009**, *131*, 14838–14843.
(13) Wang, H.; Guo, X. Q.; Zhong, R.; Hou, X. F. *J. Organomet. Chem.* **2009**, *694*, 1567–1570.
(14) Milsmann, C.; Bothe, E.; Bill, E.; Weyhermuller, T.; Wieghardt, K. *Inorg. Chem.* **2009**, *48*, 6211–6221.
(15) Stenson, P. A.; Board, A.; Marin-Becerra, A.; Blake, A. J.; Davies, E. S.; Wilson, C.; McMaster, J.; Schroder, M. *Chem.—Eur. J.* **2008**, *14*, 2564–2576.
(16) Roy, A. S.; Muresan, N.; Tuononen, H. M.; Rath, S. P.; Ghosh, P. *Dalton Trans.* **2008**, 3438–3446.
(17) Pramanik, K.; Das, U.; Adhikari, B.; Chopra, D.; Stoeckli-Evans, H. *Inorg. Chem.* **2008**, *47*, 429–438.
(18) Shin, R. Y. C.; Sim, H. S.; Goh, L. Y.; Webster, R. D. *J. Organomet. Chem.* **2007**, *692*, 3267–3276.
(19) Ghosh, P.; Begum, A.; Herebian, D.; Bothe, E.; Hildenbrand, K.; Weyhermuller, T.; Wieghardt, K. *Angew. Chem., Int. Ed.* **2003**, *42*, 563–567.
(20) Kimura, S.; Bill, E.; Bothe, E.; Weyhermuller, T.; Wieghardt, K. *J. Am. Chem. Soc.* **2001**, *123*, 6025–6039.
(21) Ashby, M. T.; Enemark, J. H.; Lichtenberger, D. L. *Inorg. Chem.* **1988**, *27*, 191–197.
(22) Grapperhaus, C. A.; Mullins, C. S.; Kozlowski, P. M.; Mashuta, M. S. *Inorg. Chem.* **2004**, *43*, 2859–2866.
(23) Grapperhaus, C. A.; Mullins, C. S.; Mashuta, M. S. *Inorg. Chim. Acta* **2005**, *358*, 623–632.
(24) Mullins, C. S.; Grapperhaus, C. A.; Kozlowski, P. M. *J. Biol. Inorg. Chem.* **2006**, *11*, 617–625.
(25) Walling, C.; Helmreich, W. *J. Am. Chem. Soc.* **1958**, *81*, 1144–1148.
(26) Chatgilialoglu, C.; Ferreri, C.; Ballestri, M.; Mulazzani, Q. G.; Landi, L. *J. Am. Chem. Soc.* **2000**, *122*, 4593–4601.
(27) Ichinose, Y.; Oshima, K.; Utimoto, K. *Chem. Lett.* **1988**, 669–672.
(28) Lalevee, J.; Allonas, X.; Fouassier, J. P. *J. Org. Chem.* **2006**, *71*, 9723–9727.
(29) Wang, K.; Stiefel, E. I. *Science* **2001**, *291*, 106–109.
(30) Harrison, D. J.; Nguyen, N.; Lough, A. J.; Fekl, U. *J. Am. Chem. Soc.* **2006**, *128*, 11026–11027.
(31) Geiger, W. E. *Inorg. Chem.* **2002**, *41*, 136–139.
(32) Harrison, D. J.; Lough, A. J.; Nguyen, N.; Fekl, U. *Angew. Chem., Int. Ed.* **2007**, *46*, 7644–7647.
(33) Kerr, M. J.; Harrison, D. J.; Lough, A. J.; Fekl, U. *Inorg. Chem.* **2009**, *48*, 9043–9045.
(34) Shin, R. Y. C.; Teo, M. E.; Leong, W. K.; Vittal, J. J.; Yip, J. H. K.; Goh, L. Y.; Webster, R. D. *Organometallics* **2005**, *24*, 1483–1494.
(35) Dilworth, J. R.; Hutson, A. J.; Morton, S.; Harman, M.; Hursthouse, M. B.; Zubieta, J.; Archer, C. M.; Kelly, J. D. *Polyhedron* **1992**, *11*, 2151–2155.
(36) Dilworth, J.; Zheng, Y.; Lu, S.; Wu, Q. *Trans. Met. Chem.* **1992**, *17*, 364–368.
(37) Grapperhaus, C. A.; Poturovic, S. *Inorg. Chem.* **2004**, *43*, 3292–3298.
(38) Grapperhaus, C. A.; Poturovic, S.; Mashuta, M. S. *Inorg. Chem.* **2002**, *41*, 4309–4311.
(39) Grapperhaus, C. A.; Kozlowski, P. M.; Kumar, D.; Frye, H. N.; Venna, K. B.; Poturovic, S. *Angew. Chem., Int. Ed.* **2007**, *46*, 4085–4088.
(40) Grapperhaus, C. A.; Poturovic, S.; Mashuta, M. S. *Inorg. Chem.* **2005**, *44*, 8185–8187.
(41) Grapperhaus, C. A.; Venna, K. B.; Mashuta, M. S. *Inorg. Chem.* **2007**, *46*, 8044–8050.
(42) Poturovic, S.; Grapperhaus, C. A.; Mashuta, M. S. *Angew. Chem., Int. Ed.* **2005**, *44*, 1883–1887.
(43) Musie, G.; Reibenspies, J. H.; Darensbourg, M. Y. *Inorg. Chem.* **1998**, *37*, 302–310.
(44) Farmer, P. J.; Reibenspies, J. H.; Lindahl, P. A.; Darensbourg, M. Y. *J. Am. Chem. Soc.* **1993**, *115*, 4665–4674.
(45) Dilworth, J. R.; Lu, C. Z.; Miller, J. R.; Zheng, Y. F. *J. Chem. Soc., Dalton Trans.* **1995**, 1957–1964.
(46) Farrugia, L. J. *J. Appl. Crystallogr.* **1997**, *30*, 565.
(47) Tedder, J. M. *Angew. Chem., Int. Ed. Engl.* **1982**, *21*, 401–410.
(48) *DigiSim* (3.03b); Bioanalytical Systems, Inc.: West Lafayette, IN, 2004.
(49) Sakurai, H.; Hayashi, S.; Hosomi, A. *Bull. Chem. Soc. Jpn.* **1971**, *44*, 1945–1949.
(50) Jones, M. J.; Moad, G.; Rizzardo, E.; Solomon, D. H. *J. Org. Chem.* **1989**, *54*, 1607–1611.
(51) Mullen, G. E. D.; Blower, P. J.; Price, D. J.; Powell, A. K.; Howard, M. J.; Went, M. J. *Inorg. Chem.* **2000**, *39*, 4093–4098.
(52) Maurer, P.; Magistrato, A.; Rothlisberger, U. *J. Phys. Chem. A* **2004**, *108*, 11494–11499.
(53) Magistrato, A.; Maurer, P.; Fässler, T.; Rothlisberger, U. *J. Phys. Chem. A* **2004**, *108*, 2008–2013.
(54) Grapperhaus, C. A.; Ouch, K.; Mashuta, M. S. *J. Am. Chem. Soc.* **2009**, *131*, 64–65.
(55) *CrysAlis PRO* (CCD and RED; 1.171.34.36): Oxford Diffraction Ltd.: Yarnton, England, 2010.

(56) Sheldrick, G. M. *Acta Crystallogr.* **1990**, *A46*, 467.
(57) *SHELXL-97*; University Gottingen: Gottingen, Germany, 1997.
(58) *SHELXTL* (v6.14); Bruker Advanced X-ray Solutions, Inc.: Madison, WI, 2000.
(59) Altomare, A.; Burla, M. C.; Camalli, M.; Cascarano, G. L.; Giacovazzo, C.; Guagliardi, A.; Moliterni, A. G. G.; Polidori, G.; Spagna, R. *J. Appl. Crystallogr.* **1999**, *32*, 115–119.